arXiv:astro-ph/0008284v1 18 Aug 2000

Construction and Testing of a Pixellated CZT Detector and Shield for a Hard X-ray Astronomy Balloon Flight

P. F. Bloser, T. Narita, J. A. Jenkins, and J. E. Grindlay

Harvard-Smithsonian Center for Astrophysics, 60 Garden St., Cambridge, MA 02138, USA

ABSTRACT

We report on the construction and laboratory testing of pixellated CZT detectors mounted in a flip-chip, tiled fashion and read out by an ASIC, as required for proposed hard X-ray astronomy missions. Two 10 mm × 10 mm × 5 mm detectors were fabricated, one out of standard eV Products high-pressure Bridgman CZT and one out of IMARAD horizontal Bridgman CZT. Each was fashioned with a 4 × 4 array of gold pixels on a 2.5 mm pitch with a surrounding guard ring. The detectors were mounted side by side on a carrier card, such that the pixel pitch was preserved, and read out by a 32-channel VA-TA ASIC from IDE AS Corp. controlled by a PC/104 single-board computer. A passive shield/collimator surrounded by plastic scintillator encloses the detectors on five sides and provides a $\sim 40^\circ$ field of view. Thus this experiment tests key techniques required for future hard X-ray survey instruments. The experiment was taken to Ft Sumner, NM in May 2000 in preparation for a scientific balloon flight aboard the joint Harvard-MSFC EXITE2/HERO payload. Although we did not receive a flight opportunity, and are currently scheduled to fly in September 2000, we present our calibration data in the flight configuration together with data analysis techniques and simulations of the expected flight background spectrum.

Keywords: CZT, background, shielding, balloon flights, hard X-ray astronomy, instrumentation

1. INTRODUCTION

It has been more than twenty years since the last all-sky hard X-ray (> 20 keV) survey was performed by the HEAO A-4 instrument.[1] A new survey, performed with a high-sensitivity imaging instrument, is urgently needed. Cadmium Zinc Telluride (CZT) will almost certainly be the detector material that finally makes this new survey a reality. CZT offers far better energy resolution than scintillator detectors such as NaI and CsI, and the use of pixel or strip electrode readouts allows far better spatial resolution. Response up to 600 keV is possible with moderate thicknesses (5 mm) due to the high stopping power of CZT, and no cryogenic cooling is required due to its wide bandgap. Based on these advantages, CZT has already been selected for its first space-based application as a gamma-ray burst monitor on the SWIFT mission.[2] Our Harvard group has been developing more advanced CZT detectors for astronomy applications, motivated by the requirements of a wide-field, all-sky survey telescope operating between ~ 10 and 600 keV.[3,4,5,6,7,8] Specifically, we have focused on the EXIST[9] or EXIST-LITE[10] concepts as our baseline.

Before such instruments can be constructed, several technical issues remain to be addressed. Only the coded-aperture technique allows imaging between 100 keV and 600 keV, and this requires large-area, position-sensitive detectors that are subject to large background levels. For a sensitivity of ~ 0.05 mCrab, as baselined for EXIST on the International Space Station, approximately 8 m^2 of CZT are required.[9] Large fields of view (40° for each module of EXIST) are needed to conduct a survey over the entire sky, further increasing background and requiring large (1–2 mm) pixels to avoid projection effects in thick detectors. Large pixels have increased leakage current noise, and this must be reduced to allow high bias voltages for complete charge collection. The highest resistivity CZT available is high-pressure Bridgman (HPB) material. While detectors made of HPB CZT have low leakage current, they can at present only be made 10 mm × 10 mm in size with a reasonable yield, making the construction of square meter detector planes a technical challenge. Recently IMARAD Imaging Systems began producing CZT using a modified horizontal Bridgman (HB) process[11] which allows the growth of larger crystals (40 mm × 40 mm) at higher yield and thus lower cost. IMARAD CZT also appears to be more uniform than HPB material[7] which, if confirmed, makes it more suitable for large area arrays since inter-pixel calibration is less demanding. The HB CZT has a lower resistivity, however, and thus higher leakage current. We have found that appropriate contact material can reduce

Further author information: (Send correspondence to P. Bloser)
P.B.: E-mail: pbloser@cfa.harvard.edu

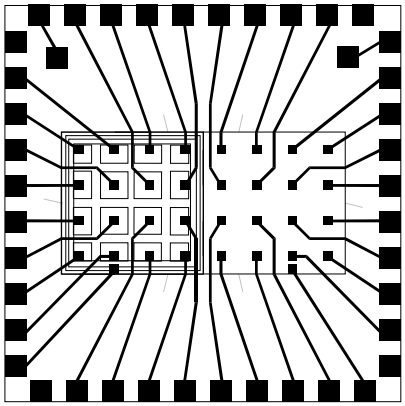

Figure 1. The Harvard flip-chip detector layout and carrier card design. Each CZT detector has a 4×4 array of pixels surrounded by a guard ring. The edge and corner pixels are made smaller to allow the pixel pitch to remain constant between detectors. The detectors are mounted side-by-side on a ceramic carrier card with gold pixel pads and traces carrying the signals to pins around the edge.

the leakage current in HB detectors to levels comparable to HPB material[7]; in particular, simple gold electrodes on IMARAD CZT act as blocking contacts and significantly reduce leakage current noise.[8]

Thus the main challenges to be addressed at present are: find a way to package small detectors that will allow them to be tiled into large arrays with a minimum of dead space; find appropriate contact materials to reduce leakage current enough to allow the use of lower-cost material; read out and process signals from thousands of pixels using low-noise ASICs that do not take up additional space; and find optimal shielding techniques to minimize the background in CZT in the high-radiation environment of low earth orbit with a minimum of mass and complexity. We have constructed a balloon experiment to test methods of meeting these challenges and to measure the spectrum and uniformity of the background generated in an imaging CZT detector. The motivation and basic design of this experiment have been described previously.[6] The completed instrument was taken to Ft. Sumner, NM in May 2000 for a balloon flight on the joint Harvard-MSFC EXITE2/HERO payload. We did not receive a flight opportunity and are currently scheduled to fly in September 2000. In this paper, therefore, we describe the completed instrument and its performance in detail and present preliminary simulations of its response and the flight background expected.

2. DESCRIPTION OF THE IMAGING CZT EXPERIMENT

The heart of the Harvard imaging CZT experiment is the tiled "array" of flip-chip-mounted pixellated detectors. This array consists of two moderately thick (10 mm $\times$ 10 mm $\times$ 5 mm) crystals, one made of HPB CZT provided by eV Products and one made of HB CZT provided by IMARAD. These crystals were fashioned into detectors with gold contacts by RMD, Inc. using a direct shadow mask and evaporator technique.[8] Gold contacts were selected for both crystals in order to make a well-understood ohmic detector out of the eV Products material and because we have found that gold contacts on IMARAD material act as blocking contacts and greatly reduce leakage current.[8] The pixel layout and tiling configuration is shown in Figure 1, along with the design of the detector carrier card. Each detector was made with a 4×4 array of pixels on a 2.5 mm pitch with 150 μm gaps, surrounded by a guard ring. The inner pixels were made 2.35 mm across, while the edge and corner pixels were made slightly smaller so that the 2.5 mm pitch could be preserved when the detectors were mounted side-by-side (Figure 1).

Both detectors were tested using a pogo pin and eV Products preamp prior to flip-chip mounting. Figure 2 shows the 32 spectra recorded in this manner using a ^{57}Co source. The top 16 spectra are from the IMARAD detector and the bottom 16 from the eV Products detector; the plots are arranged in the order of the pixels when both detectors are mounted. Data were taken from each pixel individually; the integration times were not identical and the detector had to be repositioned between each run, so the illumination was not uniform. The spectra are generally quite good, except for areas of material defects in the lower right corners of both detectors.

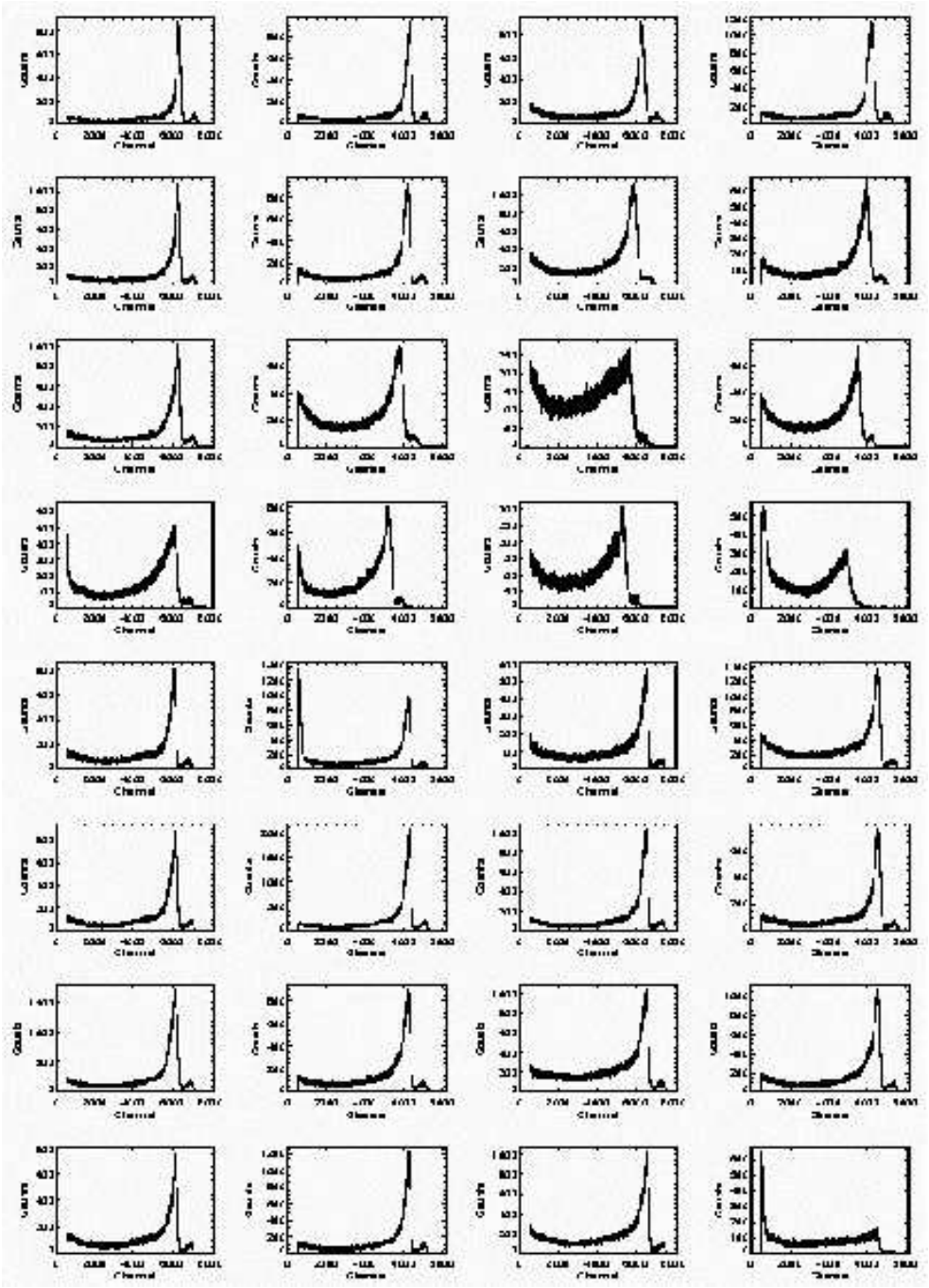

Figure 2. ^{57}Co spectra recorded in the IMARAD detector (top 4 × 4 spectra) and eV Products detector (bottom 4 × 4 spectra) prior to flip-chip mounting. Each spectrum was recorded individually using a pogo pin and eV Products preamp. The lower right corners of both detectors show bad spectra due to material defects.

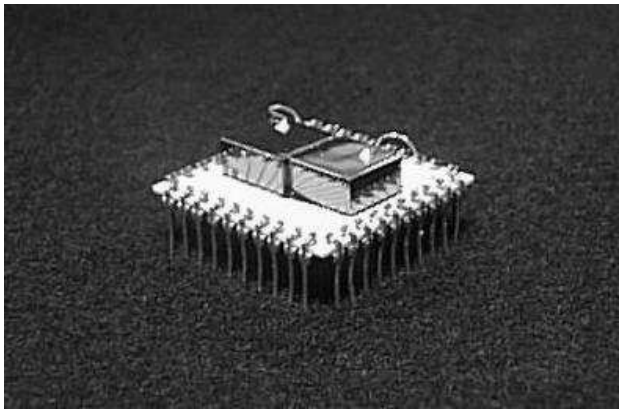

Figure 3. The two CZT detectors mounted flip-chip fashion on the ceramic carrier card. The pixel pitch is maintained across the two detectors, as required for an imaging detector array. The thin wires epoxied to the gold cathodes supply high voltage.

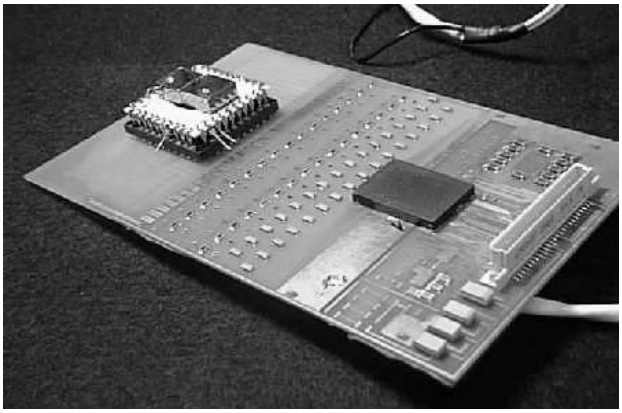

Figure 4. The custom-designed 32-channel VA-TA ASIC card, supplied by IDE AS Corp., with the flip-chip CZT detector plugged in. The VA-TA is mounted under the protective cover on the right side. The VA-TA is read out by a commercial DAQ board, which is in turn controlled by a PC/104 computer.

The two CZT detectors were mounted in a flip-chip fashion on a ceramic carrier board by HyComp, Inc. The carrier card was made with a 4×8 array of gold pixel pads on a 2.5 mm pitch, with traces running from each pad to pins on the edge (Figure 1). Additional pads were included to ground the guard rings and bring high voltage onto the card. A gold wire bond bump (~ 100 μm across) was attached to each pad and coined flat. Conductive epoxy was applied to the pads with a stencil and the detectors were aligned and mounted. After the conductive epoxy had cured a non-conductive epoxy underfill was injected under the detectors to provide mechanical strength. In Figure 3 we show the assembled flip-chip CZT detector mounted on its carrier card. Negative high voltage is applied via the two thin wires epoxied to the gold cathodes.

An second identical flip-chip detector was manufactured for us by HyComp using additional IMARAD and eV Products CZT crystals. The raw CZT material was of slightly higher quality in this second detector; however, after assembly we found that several IMARAD pixels were partially shorted to the high voltage input. As this would endanger the readout electronics, we have not proceeded with testing this detector. We report here only results for the first detector, which we will fly in September.

Both detectors are read out by a self-triggering, 32-channel VA-TA ASIC supplied by IDE AS Corp. in Norway. The CZT detector card plugs directly into a custom-designed VA-TA carrier board, as shown in Figure 4. The ASIC is read out by a commercial data acquisition (DAQ) board also supplied by IDE. This VA-DAQ board is in turn controlled by a PC/104 single-board computer running DOS software adapted by us from IDE-supplied Labview code. This code allows us to set the trigger threshold and to mask out noisy channels. The VA-TA card is a preliminary design made for our test balloon flight only; it is not suitable for our final survey telescope due to its large area and long lead lengths between detector and ASIC.

The fully-assembled CZT experiment is shown in its pressure vessel in Figure 5. The detectors are visible slightly above center. They are surrounded by a passive Pb/Sn/Cu collimator which is in turn surrounded by plastic scintillator read out by miniature PMTs (Hamamatsu R7400U, 1.5 cm diameter). The collimator provides a $40^\circ \times 40^\circ$ field of view, and the plastic scintillator will veto local gamma-rays produced in the passive material by cosmic ray interactions. A similar rear shield, not visible, sits below the CZT. (Further details of the shielding configuration have been described by us previously.[6]) The VA-TA card is enclosed in a thin aluminum shield box to isolate it electrically from the rest of the hardware; we have found that the ASIC is extremely susceptible to ground loop and pickup noise. At the bottom of the figure is the PC/104 computer that controls the data acquisition, reading out all 32 channels for each trigger. The PC/104 stack includes an analog/digital I/O card (DM5408) that allows the computer to set thresholds for the PMTs, switch the CZT and PMT high voltage on and off, and monitor coincident CZT and plastic shield events. The coincidence electronics are enclosed in the box at left. Computer and other electronic power is distributed in the boxes on the right. Not visible is the compact high voltage supply (C12N)

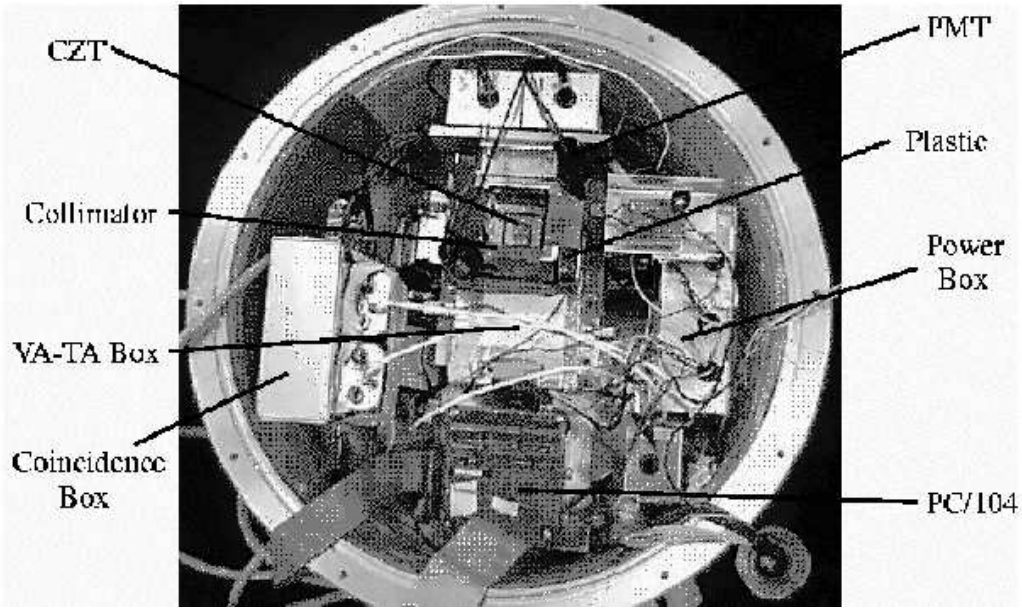

Figure 5. The complete Harvard CZT experiment in its pressure vessel, looking down the collimator at the CZT detectors. Visible are the passive collimator with its surrounding plastic scintillator and readout PMTs, the VA-TA shield box, the PC/104 computer, shield coincidence logic electronics box, and power regulation boxes. The experiment is scheduled to fly from Ft. Sumner, NM in September 2000.

provided by EMCO High Voltage Corp. Normal operating bias for the CZT detectors is -500 V. The ASIC and high voltage supply are powered by isolated batteries, which we have found to be critical for low-noise operation. A temperature sensor is included and read out by the PC/104. In normal operating mode the PC/104 collects events for one second, recording all 32 channels and the plastic shield flags for each event, and packages them into a buffer with the housekeeping data. These buffers are sent out to the main EXITE2/HERO data stream via the serial port. We are limited by overall balloon system throughput requirements to 50 CZT events per buffer.

3. CZT DETECTOR TESTING AND DATA ANALYSIS

The leakage current was measured as a function of bias voltage for both detectors for each pixel. The voltage was varied between -600 V and +200 V. It was immediately obvious that three pixels on the IMARAD detector were shorted to ground. The pins connected to these pixels were lifted so as not to connect to the ASIC. It is not clear why this happened only on the IMARAD side; we suspect that the non-conductive underfill epoxy reacted differently with the IMARAD material than with the eV Products material, perhaps creating a conducting oxide layer that led to shorts. The leakage current on the other pixels was fairly uniform, with values of $\sim$ 1–2 nA per pixel at -500 V for both detectors.

Calibration spectra were taken by fully illuminating both detectors simultaneously using ^{241}Am and ^{57}Co sources. The ASIC trigger threshold was set at $\sim$ 30 keV. We discovered that two channels on the eV Products detector were dead, and that six additional IMARAD pixels were too noisy to use with our 50 cts buffer^{-1} limitation. These pixels were mostly on the far side of the IMARAD detector from the VA-TA chips and therefore had the longest traces on the VA-TA card. We masked these channels out.

The spectra in the remaining 21 channels were acceptable, but could be greatly improved through simple data post-processing. The spectral degradation was due to charge-sharing between pixels for events that occurred near pixel boundaries. Since our pixels are quite large, charge is only shared between two pixels in most cases. We therefore adopted the following procedure: 1) We first performed a rough energy calibration on each channel using the 60 keV line from ^{241}Am and 122 keV line from ^{57}Co. 2) For each event, we found the channel containing the largest pulse height. The photon presumably interacted in this pixel. 3) We searched the surrounding 4 "nearest

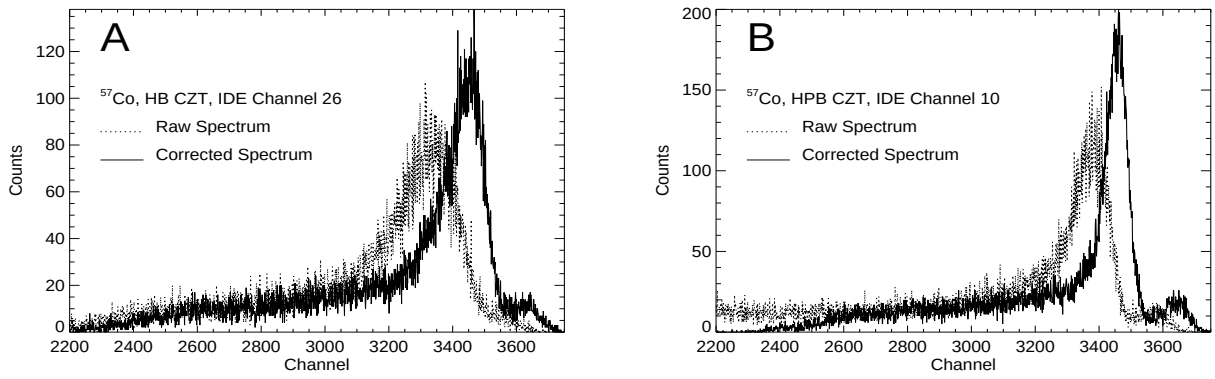

Figure 6. A) Improvement in an IMARAD pixel (IDE channel 26) ^{57}Co spectrum due to data post-processing. The energy resolution improves from 15.6% to 10.2%. B) Improvement in an eV Products pixel (IDE channel 10) spectrum due to post-processing. The energy resolution improves from 8.9% to 5.2%.

neighbor" pixels for the maximum pulse height. This is the pixel into which charge may have been shared. 4) The pulse height from the neighbor pixel is adjusted by the relative gain and offset and added to the pulse height of the central pixel. Thus each event is corrected for charge loss due to sharing between pixels.

The improvement in our ^{57}Co spectra due to our data processing is shown in Figure 6. Both an IMARAD HB CZT pixel and an eV Products HPB CZT pixel are shown. The raw spectrum is shown by the dotted line, and the corrected spectrum by the solid line. In both cases the energy resolution E_{res} improves dramatically: from 15.6% to 10.2% on the IMARAD pixel and from 8.9% to 5.2% on the eV Products pixel. Charge sharing between pixels is clearly an important effect even with large 2.35 mm pixels.

The corrected ^{57}Co spectra for all working pixels are shown in Figure 7. The spectra are arranged so that the ASIC would sit at the bottom of the figure. It is apparent that the noisy IMARAD pixels are located on the far side of the detector from the ASIC and so suffer from long lead lengths. Our final intended detector-ASIC coupling scheme would eliminate this problem by placing the ASIC inputs directly below the pixels. The remaining IMARAD channels happen to correspond to those pixels with poor material qualities, as shown in Figure 2, with the exception of one good pixel on the left edge. Thus the average of the energy resolution values on the IMARAD detector, with its standard deviation, is $\bar{E}_{res} = (16 \pm 9)\%$, comparable to scintillator detectors.

The spectra on the eV Products side of the detector are quite good. The variations in the number of counts are due partly to material variations and partly to uneven illumination from the narrow beam of our ^{57}Co source. The average energy resolution on the eV Products detector is $\bar{E}_{res} = (7.3 \pm 2.8)\%$; this number drops to $\bar{E}_{res} = (6.7 \pm 1.2)\%$ if the lower right pixel, shown in Figure 2 to be bad, is excluded. These spectra are the best that we have seen published from a CZT detector, read out by an ASIC, in a fully flight-ready configuration.

4. DETECTOR SIMULATIONS AND PREDICTED BACKGROUND

We have carried out preliminary simulations of the tiled CZT detector to determine its response and predict the expected flight background spectrum and uniformity. These simulations were performed in two parts. First, the propagation of X-ray photons in the experiment materials and their interaction in the detector were simulated using MGEANT.[12] MGEANT is an improved user interface to the CERN Program Library Monte Carlo simulation package GEANT, allowing the easy specification of detector materials and geometry as well as the input particle spectrum and distribution. For every event interacting in the CZT the energy deposited and the location were recorded. All relevant physical processes, including photoelectric absorption, Compton scattering, and pair production, were included.

Second, the charge transport and signal induction on the pixels were calculated. We followed a procedure similar to that given by Kalemci et al.[13] First the electric field $\vec{E}$ and weighting potential[14] W_{pot} were calculated for our

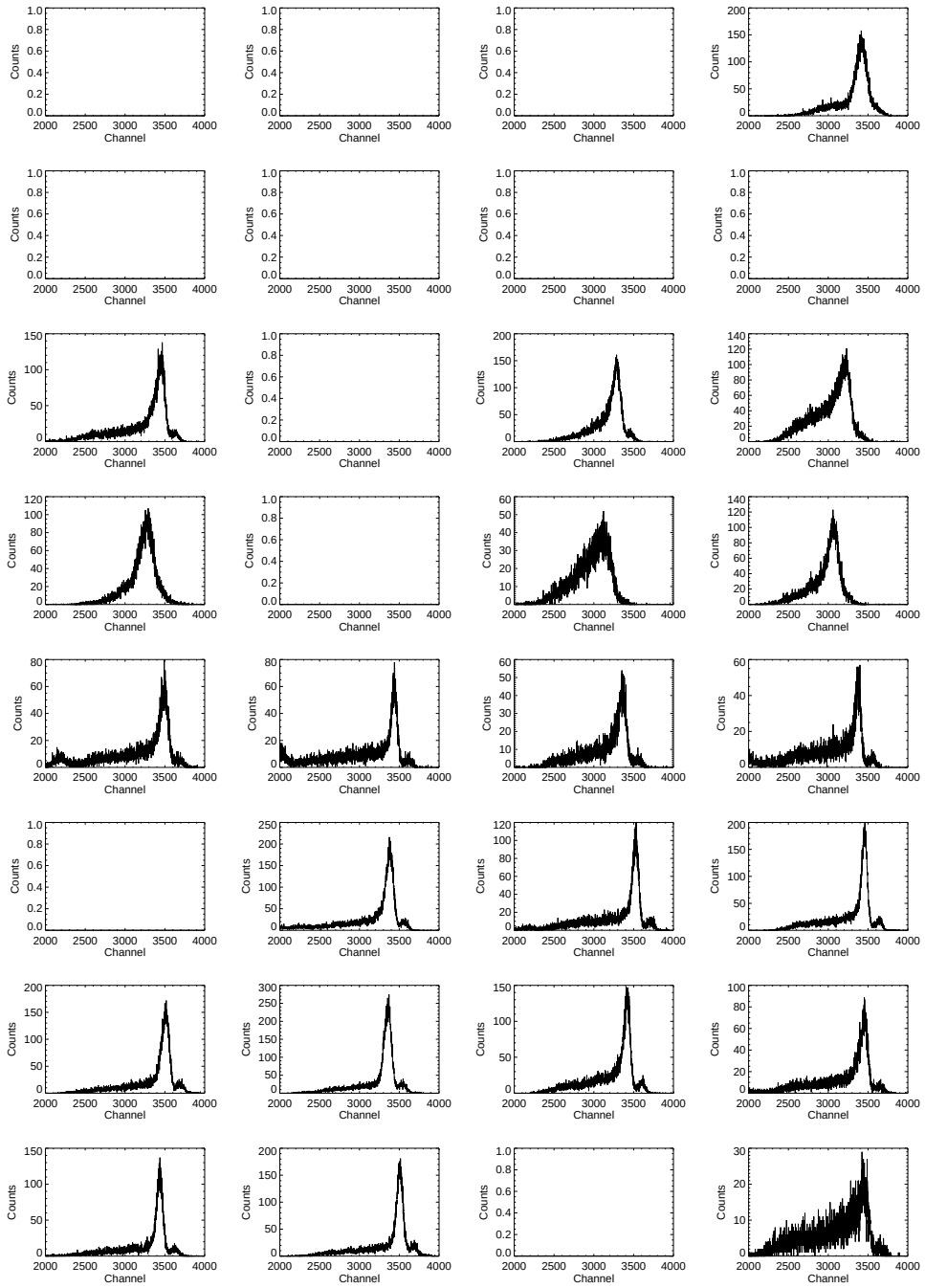

Figure 7. Corrected ^{57}Co spectra in all working pixels of the imaging CZT experiment. The IMARAD detector makes up the top 4×4 plots and the eV Products detector the bottom 4×4 plots. The plots are arranged so that the VA-TA ASIC sits below the figure. The noisy channels on the IMARAD detector, at the top of the figure, are on the far side from ASIC and so have the longest lead lengths. The good IMARAD channels happen to correspond to bad pixels due to material defects (see Figure 2) with the exception of one good pixel on the left edge. $\bar{E}_{res} = (16 \pm 9)\%$ for the IMARAD detector and $\bar{E}_{res} = (7.3 \pm 2.8)\%$ for the eV Products detector.

pixel geometry using the commercial electrostatics program ES3. The electric field calculation assumed 500 V on the cathode and 0 V on the pixels, while the weighting potential calculation assumed a potential of 1 on the pixel of interest and 0 on all other electrodes. The values of $\vec{E}$ and W_{pot} were calculated on a 5 μm grid. We used only a two-dimensional slice through the center of an inner pixel for the present simulations; the interaction positions given by MGEANT were therefore collapsed into two dimensions. Charges were then propagated along the grid one step at a time, according to the components E_z and E_x of the electric field. For each step the charge Q_{ind} induced on the pixel is given by the incremental change in the weighting potential[14]:

$$Q_{ind} = Q_{drift} \times \Delta W_{pot}, \tag{1}$$

where Q_{drift} is the total of the charges drifting along $\vec{E}$. The number of drifting charges will gradually decrease due to trapping. We employed a simple exponential expression to describe the amount of charge Q'_{drift} that arrives at each point in the grid due to trapping at the previous point[13]:

$$Q'_{drift} = Q_{drift} e^{-L_{drift}/L_{trap}}, \tag{2}$$

where L_{drift} is the distance drifted between grid points and the trapping length L_{trap} is given by

$$L_{trap} = \mu\tau (E_x^2 + E_z^2)^{1/2}, \tag{3}$$

where $\mu\tau$ is the product of the charge carrier mobility and lifetime. The charge clouds were assumed to be points with no diffusion. Each cloud was followed until it reached an electrode and the total induced charge for that event was tabulated. The resulting histogram of detector pulse heights was finally convolved with a gaussian to simulate electronic noise.

We first used MGEANT to illuminate the CZT detectors with a simulated ^{57}Co spectrum to compare with our calibration data. Both recorded and simulated spectra were fit with a combination of a gaussian photopeak and an exponential tail to determine E_{res} and the photopeak efficiency.[5] The photopeak efficiency is defined as the ratio of the photopeak counts to the total counts within a range around the gaussian center from -4σ to $+2.35\sigma$. The electron mobility-lifetime product $\mu_e\tau_e$ has been well-measured in HPB CZT,[15] and we fixed this quantity at a typical value of 3×10^{-3} cm^2 V^{-1}. (Our previous work indicates similar $\mu_e\tau_e$ values in IMARAD material.[7]) The hole mobility-lifetime product $\mu_h\tau_h$ and convolving gaussian width σ at 122 keV were then adjusted to generate the best match in energy resolution and photopeak efficiency to the recorded data. We found the best agreement for values of $\mu_h\tau_h = 10^{-6}$ cm^2 V^{-1} and $\sigma = 2.5$ keV. This value of $\mu_h\tau_h$ is somewhat lower than typical values found in the literature.[16] In Figure 8 we show the corrected ^{57}Co spectrum recorded from an inner pixel of the eV Products HPB detector together with our simulated ^{57}Co spectrum using these parameters. The recorded spectrum has an energy resolution of 7.3% and a photopeak efficiency of 84%. The simulated spectrum has an energy resolution of 7.6% and a photopeak efficiency of 75%. It is obvious that the photopeak is accurately reproduced, but not the tail, which in the real data extends to lower energies with a flatter slope. This could be due to additional trapping in the corners of the pixel, which is not included in our two-dimensional model. Assuming that the average electron-hole pair creation energy is 4.6 eV,[17] the 2.5 keV gaussian width corresponds to an equivalent noise of ~ 540 e^-, compared to the 300 e^- noise that the VA-TA system should provide under ideal conditions. The difference is likely due to capacitance effects from the long lead lengths.

Using the parameters given above for the CZT detector response, we have simulated the expected background spectrum in one inner pixel at our planned balloon float altitude, corresponding to 3.5 g cm^{-2} residual atmosphere. A model of the aluminum pressure vessel and internal hardware was created using MGEANT, along with the Pb/Sn/Cu passive collimator and shield. The pressure vessel was irradiated with the measured atmospheric gamma-ray spectrum between 20 keV and 10 MeV,[18] assumed here to be isotropic. The resulting spectrum in one pixel of the CZT is shown in Figure 9. This spectrum represents a best case, assuming that the plastic scintillator shields veto all local gamma-ray production from charged particles. The spectrum has been convolved with a gaussian whose width varies according to $\sigma = 2.5(E/122\text{keV})^{1/2}$ keV. The background level at 100 keV is $\sim 3.6 \times 10^{-3}$ cts cm^{-2} s^{-1} keV^{-1}.

For comparison, we have plotted in Figure 10 the predicted background together with the results of several CZT balloon experiments. Since most previous balloon flights have involved 2 mm thick detectors, we plot the backgrounds per detector volume. Several experiments used only passive shielding: the first flight of the Goddard Space Flight Center experiment PoRTIA,[19] with 2 mm Pb shielding around a 25.4 mm $\times$ 25.4 mm $\times$ 1.9 mm

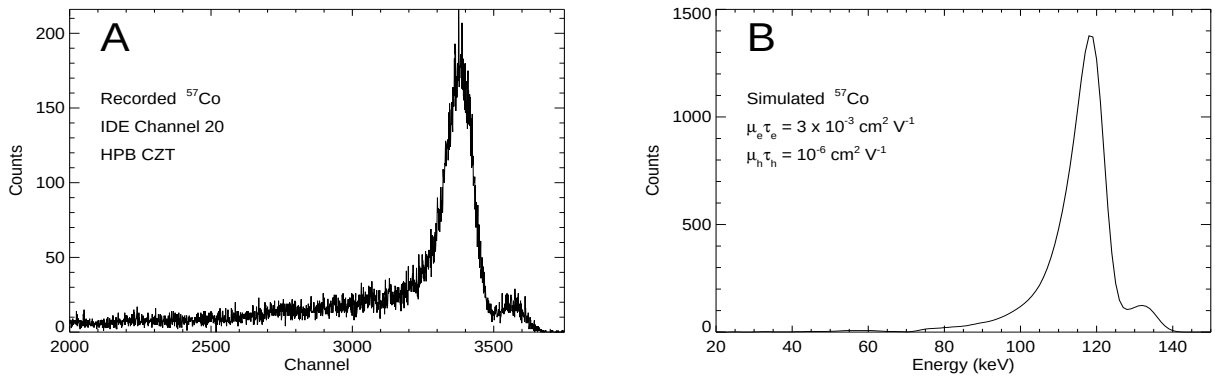

Figure 8. A) Recorded ^{57}Co spectrum from IDE channel 20, an inner pixel of the eV Products detector. Here E_{res} = 7.3% and photopeak efficiency = 84%. B) Simulated ^{57}Co spectrum using $\mu_e\tau_e = 3 \times 10^{-3}$ cm^2 V^{-1}, $\mu_h\tau_h = 10^{-6}$ cm^2 V^{-1}, and σ = 2.5 keV. This corresponds to an electronic noise of $\sim 540\ e^-$. The simulation mimics the photopeak quite well, but does not reproduce the tail completely. Here $E_{res} = 7.6\%$ and photopeak efficiency = 75%.

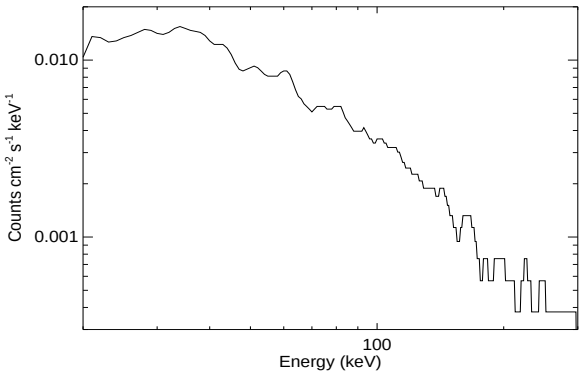

Figure 9. Predicted background at 3.5 g cm^{-2} residual atmosphere for the imaging CZT detector. Only photon interactions are included and the plastic scintillator is assumed to veto all local gamma production. The background at 100 keV is $\sim 3.6 \times 10^{-3}$ cts cm^{-2} s^{-1} keV^{-1}.

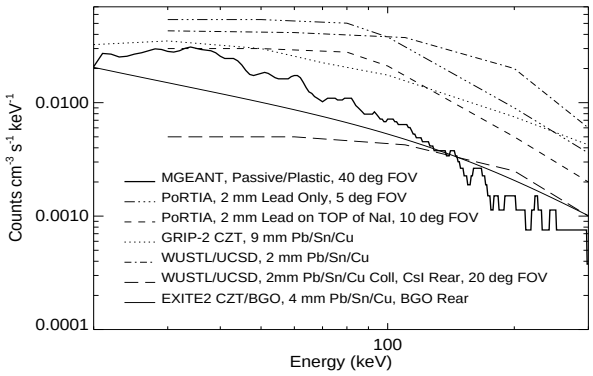

Figure 10. Comparison of our predicted background with previous measurements, plotted per detector volume to account for different detector thicknesses. The predicted level is lower than that in totally passive experiments, and comparable to that in experiments employing some active shielding.

detector and a 5° field of view, the Caltech CZT detector flown on the GRIP-2 payload,[20] with 9 mm of graded Pb, Sn, and Cu completely shielding a 10 mm × 10 mm × 2 mm detector, and the first flight of the Washington University, St. Louis and University of California-San Diego (WUSTL/UCSD) cross-strip detector,[21] with 2 mm of graded Pb, Sn, and Cu completely surrounding a 12 mm × 12 mm × 2 mm employing orthogonal strips electrodes for readout. The backgrounds recorded by these experiments are all higher than that expected from our tiled CZT detectors, due mainly to the local production of gamma-rays in the passive shielding by cosmic-ray interactions. Other previous experiments have used partial active shielding: the second flight of PoRTIA,[19] in which the detector was placed on top of a large NaI crystal (now with a 10° field of view), the second flight of the WUSTL/UCSD detector,[22] which employed a 2 mm Pb/Sn/Cu collimator with a 20° field of view and a rear CsI shield, and our previous CZT experiment flown on EXITE2,[4] which completely enclosed a 10 mm × 10 mm × 2 mm CZT detector in 4 mm of Pb/Sn/Cu in the front and a thick BGO shield in the rear. The active/passive WUSTL/UCSD and EXITE2 CZT/BGO background levels are comparable to the predicted tiled detector background, though lower at

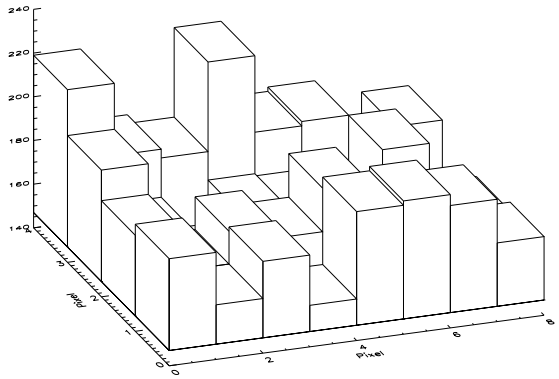

Figure 11. Predicted uniformity of the flight background from MGEANT simulations. Plotted are the total counts recorded in each pixel. The edge pixels have generally higher background rates, as expected, though the significance is low.

low energies due to their smaller fields of view. It is not clear why the active/passive PoRTIA spectrum is still so high; perhaps the solid angle subtended by the NaI shield was not sufficient to veto local gammas. The previous experiments clearly demonstrate that at least partial active shielding is required to achieve low background levels. The second WUSTL/USCD flight showed in addition that most of the background reduction was achieved with the active shield threshold set near 10 MeV, appropriate for rejecting charged particles.[22] This implies that CZT internal gamma-ray background is of secondary importance, and that our plastic shielding scheme should indeed produce the background level predicted. We will be able to test this hypothesis on our September flight: we are re-flying the CZT/BGO detector alongside the tiled detectors to compare shielding configurations,[6] and will take data with the BGO threshold set near 50 keV (to veto gamma-rays) and near 1 MeV (to veto charged particles only) to see if the gamma-ray rejection is needed.

The expected uniformity of the flight background as given by the MGEANT simulation is shown in Figure 11. We plot here the total counts recorded in each pixel. As might be expected, the background level in the inner pixels is generally lower due to shielding from the outer pixels; this difference is only about 10% on average however, and the significance is only $\sim 1\sigma$.

5. CONCLUSIONS AND FUTURE WORK

We have constructed an imaging CZT detector that demonstrates a number of the techniques required for a hard X-ray survey telescope such as that needed for EXIST. These techniques include the use of thick pixellated detectors with blocking contacts, flip-chip mounting, tiled detector geometry, ASIC readout, and shielding. The spectra recorded by the eV Products detector, on the short-lead-length side of the detector array, are the best we have seen for a CZT detector read out by an ASIC in a flight-ready configuration. Our immediate goal is to finally fly this experiment on the EXITE2/HERO balloon payload from Ft. Sumner, NM in September 2000. Our future work will include the design of an optimized ASIC and coupling scheme to minimize lead lengths (ideally coupling the ASIC directly to the CZT pixels), the improvement of our flip-chip processing, and the refinement of our detector simulations to include three-dimensions and more complicated trapping-detrapping effects. Using what we learn from the September flight we will begin the development of EXIST-LITE, a proposed ultra-long-duration balloon hard X-ray telescope employing ~ 1 m^2 of CZT to conduct a preliminary survey of half the sky.

ACKNOWLEDGMENTS

We thank S. Sansone and L. Knowles for machining work and J. Gomes, G. Nystrom, and F. Licata for engineering assistance. We also thank K. Shah and P. Bennett at RMD, Inc. for their assistance in fabricating the detectors

and G. Riley at HyComp, Inc. for his help in the flip-chip processing. We especially thank B. Sundal at IDE AS for extensive help with the VA-DAQ system. This work was supported in part by NASA grants NAG5-5103 and NAG5-5209. P. Bloser acknowledges partial support from NASA GSRP grant NGT5-50020.

REFERENCES

1. A. M. Levine et al., "The HEAO 1 A-4 catalog of high energy X-ray sources," *Astrophys. Jour. Suppl. Ser.* **54**, p. 581, 1984.
2. S. D. Barthelmy, "Burst alert telescope (BAT) on the Swift MIDEX mission," in *X-ray and Gamma-ray Instrumentation for Astronomy XI*, K. A. Flanagan and O. H. W. Siegmund, eds., *Proc. SPIE* **4140**, 2000.
3. P. Bloser, T. Narita, J. Grindlay, and K. Shah, "Prototype imaging Cd-Zn-Te array detector," in *Semiconductors for Room-Temperature Radiation Detector Applications II*, R. James, T. Schlesinger, P. Siffert, M. Cuzin, M. Squillante, and W. Dusi, eds., *Proc. MRS* **487**, p. 153, 1998.
4. P. Bloser, J. Grindlay, T. Narita, and F. Harrison, "CdZnTe background measurement at balloon altitudes with an active BGO shield," in *EUV, X-ray, and Gamma-ray Instrumentation for Astronomy IX*, O. H. W. Siegmund and M. Gummin, eds., *Proc. SPIE* **3445**, p. 186, 1998.
5. T. Narita, P. Bloser, J. Grindlay, R. Sudharsanan, C. Reiche, and C. Stenstrom, "Development of prototype pixellated PIN CdZnTe detectors," in *Hard x-ray and gamma-ray detector physics and applications*, F. P. Doty and R. B. Hoover, eds., *Proc. SPIE* **3446**, p. 218, 1998.
6. P. F. Bloser, J. E. Grindlay, T. Narita, and J. A. Jenkins, "Design and testing of a prototype pixellated CZT detector and shield for hard X-ray astronomy," in *EUV, X-ray, and Gamma-ray Instrumentation for Astronomy X*, O. H. W. Siegmund and K. A. Flanagan, eds., *Proc. SPIE* **3765**, p. 388, 1999.
7. T. Narita, P. F. Bloser, J. E. Grindlay, J. A. Jenkins, and H. W. Yao, "Development of IMARAD CZT detectors with PIN contacts," in *Hard X-ray, Gamma-ray, and neutron detector physics*, R. B. James and R. C. Schirato, eds., *Proc. SPIE* **3768**, p. 55, 1999.
8. T. Narita, P. F. Bloser, J. E. Grindlay, and J. A. Jenkins, "Development of gold contacted flip-chip detectors with IMARAD CZT," in *Hard X-ray, Gamma-ray, and neutron detector physics II*, R. B. James and R. C. Schirato, eds., *Proc. SPIE* **4141**, 2000.
9. J. Grindlay et al., "EXIST: a high sensitivity hard X-ray imaging sky survey mission for ISS," in *The Fifth Compton Symposium*, M. C. McConnell and J. M. Ryan, eds., *AIP Conf. Proc.* **510**, p. 784, 2000.
10. J. Grindlay, "Balloon-borne hard x-ray imaging and future surveys," *Adv. Space Res.* **21**, p. 999, 1998.
11. P. Cheuvart, U. El-Hanany, D. Schneider, and R. Triboulet, "CdTe and CdZnTe crystal growth by horizontal Bridgman technique," *J. Crystal Growth* **101**, p. 270, 1990.
12. S. J. Sturner, H. Seifert, C. Shrader, and B. J. Teegarden, "MGEANT - a GEANT-based multi-purpose simulation package for gamma-ray astronomy missions," in *The Fifth Compton Symposium*, M. C. McConnell and J. M. Ryan, eds., *AIP Conf. Proc.* **510**, p. 814, 2000.
13. E. Kalemci, J. L. Matteson, and R. T. Skelton, "Model calculations of the response of CZT strip detectors," in *Hard X-ray, Gamma-ray, and neutron detector physics*, R. B. James and R. C. Schirato, eds., *Proc. SPIE* **3768**, p. 360, 1999.
14. S. Ramo, "Currents induced by electron motion," *Proc. I. R. E.* **27**, p. 584, 1939.
15. Z. He, G. F. Knoll, and D. K. Knoll, "Direct measurement of electron drift parameters of wide band gap semiconductors," *Nuc. Inst. Meth. A* **411**, p. 114, 1998.
16. Y. Eisen and A. Shor, "CdTe and CdZnTe room temperature x-ray and gamma-ray detectors and imaging systems," in *Semiconductors for Room Temperature Radiation Detector Applications II*, R. B. J. et al., ed., *Proc. MRS* **487**, p. 129, 1997.
17. E. Muller, M. Jung, P. Fougeres, M. Hage-Ali, and P. Siffert, "Use of a Monte-Carlo code to determine in high Z semi-conductor CdTe and CZT, both carriers lifetimes and mobilities," in *Semiconductors for Room Temperature Radiation Detector Applications II*, R. B. J. et al., ed., *Proc. MRS* **487**, p. 301, 1997.
18. N. Gehrels, "Instrumental background in balloon-borne gamma-ray spectrometers and techniques for its reduction," *Nuc. Inst. Meth. A* **239**, p. 324, 1985.
19. A. Parsons, S. Barthelmy, L. Bartlett, F. Birsa, N. Gehrels, J. Naya, J. Odom, S. Singh, C. Stahle, J. Tueller, and B. Teegarden, "CdZnTe background measurements at balloon altitudes," *Proc. SPIE* **2806**, p. 432, 1996.

20. F. Harrison, C. Hailey, J. Hong, A. Wong, and W. Cook, "Background in balloon-borne hard x-ray/soft gamma-ray cadmium zinc telluride detectors," *Nuc. Inst. Meth. A* , in press.
21. K. Slavis, P. Dowkontt, F. Duttweiler, J. Epstein, P. Hink, G. Huszar, P. Leblanc, J. Matteson, R. Skelton, and E. Stephan, "High altitude balloon flight of CdZnTe detectors for high energy x-ray astronomy," in *EUV, X-ray, and Gamma-ray Instrumentation for Astronomy IX*, O. H. W. Siegmund and M. Gummin, eds., *Proc. SPIE* **3445**, p. 169, 1998.
22. K. Slavis, P. Dowkontt, F. Duttweiler, J. Epstein, P. Hink, G. Huszar, P. Leblanc, J. Matteson, R. Skelton, and E. Stephan, "High altitude balloon flight of CdZnTe detectors for high energy x-ray astronomy part ii," in *EUV, X-ray, and Gamma-ray Instrumentation for Astronomy X*, O. H. W. Siegmund and K. A. Flanagan, eds., *Proc. SPIE* **3765**, p. 388, 1999.